Journal of Electronic Packaging, September 2008
J. Electron. Packag. **130**, 031002 (2008) *(10 pages)*

An Investigation Into the Effect of the PCB Motion on the Dynamic Response of MEMS Devices Under Mechanical Shock Loads

Fadi Alsaleem
Mohammad I. Younis

e-mail: myounis@binghamton.edu

Ronald Miles

Department of Mechanical Engineering, State University of New York at Binghamton, Binghamton, NY 13902

Received: 9 January 2007; revised: 14 January 2008; published: 29 July 2008

We present an investigation into the effect of the motion of a printed circuit board (PCB) on the response of a microelectromechanical system (MEMS) device to shock loads. A two-degrees-of-freedom model is used to model the motion of the PCB and the microstructure, which can be a beam or a plate. The mechanical shock is represented as a single point force impacting the PCB. The effects of the fundamental natural frequency of the PCB, damping, shock pulse duration, electrostatic force, and their interactions are investigated. It is found that neglecting the PCB effect on the modeling of MEMS under shock loads can lead to erroneous predictions of the microstructure motion. Further, contradictory to what is mentioned in literature that a PCB, as a worst-case scenario, transfers the shock pulse to the microstructure without significantly altering its shape or intensity, we show that a poor design of the PCB or the MEMS package may result in severe amplification of the shock effect. This amplification can cause early pull-in instability for MEMS devices employing electrostatic forces. ©2008 *American Society of Mechanical Engineers*

Contents

Background

Recently, there has been considerable interest in the reliability research on microelecromechanical system (MEMS) under shock and vibration effects. This has been boosted by the development of portable devices containing MEMS devices [1]. A MEMS device can be exposed to shock loads during fabrication, assembly process, while transporting, and in service. Short circuits, stiction, and fracture are common problems caused by mechanical shock, which lead to failure of MEMS devices [2]. A rigorous analysis of the response of MEMS devices under shock represents a key issue for their growth and commercialization.

At least four levels of assembly (packaging) can be defined in MEMS devices [3][4][5][6][7] (Fig. 1). Level 1 involves the connection between a microstructure and a substrate, Level 2 represents the bonding between the silicon substrate and a chip, Level 3 involves the connection of the leads from the chip carrier to a printed circuit board (PCB), and Level 4 represents the connection of the PCB to a supported structure. The microstructure is required to be attached to the substrate almost rigidly. This requirement is very important because sensing is usually achieved electrostatically, which is very sensitive to the substrate movement [8][9].

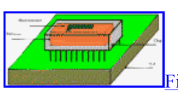
Figure 1.

Several studies have been conducted on the effect of shock loads applied directly on a MEMS device. However, less attention has been given to the shock effect on the MEMS device accounting for assembly effect. Recently, considerable research has been directed to the electronic equipment reliability under shock loads considering assembly effect. Because MEMS and electronic devices often share the same high levels of assembly (chip, PCB, and chassis) [3][4][5][6][7], it is vital to review the contributions made on the reliability of electronic devices to develop a better understanding of the MEMS response under shock loads including assembly effects. In the following we review some of the contributions in the related areas.

A.MEMS Response Under Shock Load (Without Including the Assembly Effect). Many authors have studied the MEMS response under shock loads without incorporating the assembly effect [10][11][12][13]. Wanger et al. [10], for example, studied the response of a MEMS accelerometer to a shock load induced by drop test. They used a beam theory and finite-element analysis to calculate the stress history of the device during impact. Li and Shemansky [11] solved analytically the equation of motion for the maximum deflection of a microstructure under drop test and calculated the equivalent acceleration that would cause this deflection without a drop test. De Coster et al. [12] modeled the performance of a RF MEMS switch subjected to shock using a SDOF model. They simulated the performance of the switch to minimize the insertion loss. Younis et al. [13][14] studied the combined effects of shock and electrostatics forces on MEMS devices both theoretically and experimentally. Younis et al. [15] presented computationally efficient approaches to model microstructures and microbeams under mechanical shock. Other works are reviewed in Ref. [13].

B.MEMS Response Under Shock Load (Including the Assembly Effect). Gogoi et al. [7] remarked that the fundamental frequency of the package and the whole system represented by the chip attached to the PCB should lie outside the intended operating frequency range of the MEMS structure. Srikar and Senturia [2] studied the reliability of MEMS devices subjected to shock loads. In this study they considered the first two levels of MEMS packaging (assembly): microstructure-substrate and substrate-chip levels. They mentioned that the response of the substrate for certain shock conditions can be approximated by a rigid body motion. They modeled the microstructure as an undamped 1DOF resonator attached to an accelerating base. They indicated that most MEMS devices experience the shock loads as quasistatic loads since their natural periods are much smaller than the duration of the shock loads. Srikar and Senturia [2] pointed out that the package reduces the shock load applied to the MEMS device and the worst-case scenario is to transfer this shock pulse without significantly altering its shape or intensity. In this work, however, we show that for certain package designs or shock duration values, the microstructure response might be amplified significantly because of the presence of a package or a PCB.

Jiang et al. [16] simulated the response of a high-*g* shock MEMS accelerometer using a finit-element method including the encapsulation effects. They indicated that the modal frequency of the packaging structure increases with Young's modulus of the encapsulation. Fan and Shaw [3] evaluated the dynamic response of a commercial-off-the-shelf accelerometer MEMS device under severe shock loads. They indicated that the PCB, on which the MEMS device is mounted, introduces undesirable effects on the acceleration measurements. To alleviate this factor, they proposed either to stiffen the PCB or to mount the accelerometer near a mounting position. Fan and Shaw's [3] work lacks quantitative guidelines that could be followed by a designer to eliminate the PCB effects. Shetye [17] investigated the drop test of a microphone diaphragm attached to a package. He used a 2DOF model to simulate the drop response of the system. The first DOF accounts for the diaphragm and the second degree of freedom accounts for the interaction between the package and the environment. Shetye [17] did not investigate the effect of the shock duration or the electrostatic force effect on the diaphragm response. Bart et al. [18] discussed the development of an automated package MEMS simulator, which could be used to evaluate the MEMS response under shock and thermal loads. Younis et al. [19] used a continuous-lumped mass model to simulate the PCB-MEMS assembly response under the effect of a point force impacting the PCB.

C.Electronic Equipment Response Under Shock Load. MEMS and electronic equipment commonly share similar high levels of assembly (packaging). Next we review some studies on the effect of shock loads on electronic equipment accounting for these high levels of assembly. Suhir [20] reviewed some of the works in the area of structural analysis of microelectronics and photonics. Steinberg [21] studied the effect of shock and vibration on the PCB chassis assembly used in many electronic equipment. He used a 2DOF model accounting for the chassis and the PCBs. He noticed that if the natural frequencies of the PCBs are close to that of the support chassis, their transmissibility values can be coupled, which magnifies the PCB acceleration substantially. To alleviate the coupling effect, he suggested the separation of the natural frequencies of the chassis and the various PCBs.

Suhir and Burke [22] explored the dynamic behavior of a liquid crystal display (LCD) to a shock load originated from a drop test. This LCD is packaged in a double box system (chassis and cabinet). They used a 2DOF lumped mass model and a continuous model to represent the system. To reduce the deflection of the LCD, they suggested designing the lower natural frequency of the system to be much less than the higher one. In this work, however, we show that following the above condition may lead to undesirable responses. Suhir [23] developed a mathematical model to evaluate the dynamic response of a microelectronic structure product/package to a drop and shock test. He concluded that shock test loading duration should be shorter than the period of lowest natural frequency of the system to avoid undesirable effect.

Pitarresi and Primavera [24] studied the dynamic modeling of a PCB populated with electronic components under vibration load. Suhir [25] discussed the effect of viscous damping on the displacement and acceleration of an electronic equipment package under shock load. Suhir [26] determined the maximum acceleration experienced by electronic components mounted on a PCB under shock accounting for the nonlinear dynamic effects of the PCB. Wong [27] analyzed the dynamic behavior of a PCB under a drop impact. He used a lump mass, beam, and plate models to capture the dynamic behavior of the PCB. He concluded that the PCB response depends on the ratio between the frequency of the PCB and the input shock pulse. Keltie and Falter [28] presented guidelines that could be used to simplify the shock analysis of a rigid body mounted on a beam, which is common in electronic assembly. Wong et al. [29] studied the dynamics of a PCB assembly subjected to a half-sine shock load. To improve the assembly shock reliability they suggested to use a very thin or a very a thick PCB. The readers are referred to Refs. [21][30] for more information on shock on electronic equipment.

From the aforementioned review, we first note the lack of a comprehensive study on the effect of PCB motion on the MEMS response under shock load. Only qualitative guidelines to eliminate the undesirable effect of the PCB motion on the MEMS response have been presented so far [3][7]. It is noted that also, while there are some studies on the effect of the PCB motion on the response of electronic equipment, less attention has been given to the effect of the shock duration on their response [21][31]. The main objective of the present study is to examine the effects of shock duration, damping, and electrostatic force on the response of a MEMS device based on a model that accounts for the PCB motion. Quantitative guidelines will be presented based on a case study, which could be used to element the PCB motion effect.

D.Electrostatic MEMS Devices. MEMS devices commonly involve capacitive sensing and/or actuation, in which one plate or electrode is actuated electrostatically and its motion is detected by capacitive change. There are numerous examples of MEMS devices, which depend on electrostatic excitation and detection, such as resonant microsensor, RF MEMS switches, and MEMS accelerometer devices. In this method, the driving load is the attractive force between two electrodes of a capacitor. The electrostatic load has an upper limit beyond which the mechanical restoring force of the microstructure can no longer resist its opposing electrostatic force, thereby leading to the collapse of the structure. This structural instability phenomenon is known as pull-in [32].

Problem Formulation

There are two approaches to model shock and impact on electronics devices. In one approach, a single point force is assumed to impact the PCB. Physically this could be due to a hammer hit. In the second approach the shock force is modeled as a pulse acceleration transmitted to the support of the structure, also called base excitation [33]. In this work, we consider the single impact force approach effects. The second approach will be investigated in Ref. [34].

In this investigation, we assume that both the substrate-chip and the chip-PCB assembly are rigidly connected [2][24]. Hence, the assembly effect reduces to that of the PCB motion only. We use a 2DOF model, Fig. 2, to study the assembly effect on the response of a MEMS device under shock load. The first DOF accounts for the PCB motion, which is subjected directly to the shock load. The second DOF represents the motion of the microstructure, such as a beam or a plate, which is mounted over the PCB.

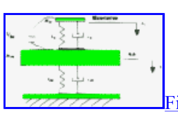
Figure 2.

Shown in Fig. 2 are the following: k_m, microstructure stiffness; k_{PC}, PCB stiffness; c_m, microstructure damping;

c_{PC}, PCB damping; m_m, microstructure mass; and m_{PC}, PCB mass. To evaluate the microstructure response under shock loads, it is assumed that the shock load is applied to the PCB directly as a single point force, the dynamic effect of the microstructure mass on the PCB is negligible, and the shock has a shape of a sine pulse of period *T*, Fig. 3, which represents a good representation for a shock pulse [35]. Under these assumptions, the governing equation of the undamped system is given by

$$\begin{bmatrix} m_m & 0 \\ 0 & m_{PC} \end{bmatrix} x'' + \begin{bmatrix} k_m & -k_m \\ -k_m & k_m + k_{PC} \end{bmatrix} x = F(t) \quad (1)$$

where $F(t)=[0,F_0[\sin(\omega_{\text{pulse}}t)u(t)+\sin(\omega_{\text{pulse}}(t-T))u(t-T)]]^{\text{tr}}$ where t is time, $u(t)$ is the unit step function, ω_{pulse} is the shock pulse frequency, and tr denotes transpose. Using modal analysis, the responses of the microstructure and the PCB are given by

$$x_i = X_i \eta_i \tag{2}$$

where x_1 is the microstructure response, x_2 is the PCB response, X_i is the ith eigenvector, and

$$\eta_i = \frac{q_i\left[\left(\sin(\omega_{\text{pulse}}t) - \frac{\omega_{\text{pulse}}}{\omega_{ni}} \sin(\omega_{ni}t)\right)u(t)\right]}{m_i(\omega_{\text{pulse}}^2 - \omega_{ni}^2)} \quad \text{for } t < T \tag{3}$$

$$\eta_i = \frac{q_i\left[\left(\sin(\omega_{\text{pulse}}t) - \frac{\omega_{\text{pulse}}}{\omega_{ni}} \sin(\omega_{ni}t)\right)u(t)\right]}{m_i(\omega_{\text{pulse}}^2 - \omega_{ni}^2)} + \frac{q_i\left[\left(\sin\ \omega_{\text{pulse}}(t-T) - \frac{\omega_{\text{pulse}}}{\omega_{ni}} \sin\ \omega_{ni}(t-T)\right)\right]}{m_i(\omega_{\text{pulse}}^2 - \omega_{ni}^2)} \quad \text{for } t > T \tag{4}$$

where $q_i=X_i^{\text{tr}}F(t)$, ω_{ni} is the modal natural frequency, and m_i is the effective mass for each modal coordinate. In this system, the undamped coupled modal frequencies (ω_1, ω_2) have approximately the same values of the uncoupled natural frequencies of the microstructure and the PCB separately. Next, we assume proportional constant damping and solve for the light damped response of the microstructure and the PCB, which yields

$$x_i = X_i \eta_{di} \tag{5}$$

where

$$\begin{aligned}\eta_{di} = {}& \frac{q_i\lambda}{m_i\lambda^2(2-\lambda^2-4\zeta^2)-1}\left[\frac{\lambda^2-1}{\lambda}\ \sin\ \omega_{\text{pulse}}t + 2\xi(\cos\ \omega_{\text{pulse}}t - e^{-\zeta\omega_i t}\ \cos\ \sqrt{1-\zeta^2}\omega_i)\right] \\ &+ \frac{F(t)\lambda}{m_i\lambda^2(2-\lambda^2-4\zeta^2)-1}\left[\frac{e^{-\zeta\omega_i t}}{\sqrt{1-\zeta^2}}(1-2\zeta^2-\lambda^2)\sin\ \sqrt{1-\zeta^2}\omega_i t\right] \quad \text{for } t < T\end{aligned} \tag{6}$$

$$\begin{aligned}\eta_{di} = {}& \frac{q_i\lambda}{m_i\lambda^2(2-\lambda^2-4\zeta^2)-1}\left[\frac{\lambda^2-1}{\lambda}\ \sin\ \omega_{\text{pulse}}t + 2\xi(\cos\ \omega_{\text{pulse}}t - e^{-\zeta\omega_i t}\ \cos\ \sqrt{1-\zeta^2}\omega_i)\right] + \frac{q_i\lambda}{m_i\lambda^2(2-\lambda^2-4\zeta^2} \\ &+ \frac{q_i\lambda}{m_i\lambda^2(2-\lambda^2-4\zeta^2)-1}\left[\frac{\lambda^2-1}{\lambda}\ \sin\ \omega_{\text{pulse}}(t-T) + 2\xi(\cos\ \omega_{\text{pulse}}(t-T) - e^{-\zeta\omega_i(t-T)}\ \cos\ \sqrt{1-\zeta^2}\omega_i)\right] \\ &+ \frac{q_i\lambda}{m_i\lambda^2(2-\lambda^2-4\zeta^2)-1}\left[\frac{e^{-\zeta\omega_i(t-T)}}{\sqrt{1-\zeta^2}}(1-2\zeta^2-\lambda^2)\sin\ \sqrt{1-\zeta^2}\omega_i(t-T)\right] \quad \text{for } t > T\end{aligned} \tag{7}$$

where $\lambda=\omega_{\text{pulse}}/\omega_i$ and ζ is the damping ratio [36].

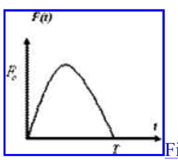

Figure 3.

Results

In this investigation, we chose a MEMS omnidirectional pressure microphone employing a microdiaphragm [37] as a case study. This diaphragm has a fundamental natural frequency ω_{MEMS} 24 kHz.

A.Undamped Response. First, we consider the undamped response of the diaphragm. This represents a worst-case scenario for the response of microstructures under shock. Figure 4(a) shows the response of the diaphragm x_1 to a shock acceleration pulse of a half-sine shape of duration T=1.0 ms using a 1DOF model of the diaphragm alone (without the PCB) [13]. The response is normalized to the static deflection of the diaphragm due to an equivalent static load F_0/k_1. It can be seen that the diaphragm responds quasistatically, since its natural period is much smaller than the duration of the shock. Next, we consider the effect of the PCB on the response. Figure 4(b) shows the normalized response of the diaphragm relative to that of the PCB x_2 using the 2DOF model. Here, the natural frequency of the PCB ω_P is chosen much less than the natural frequency of the microstructure ω_{MEMS}. Here, the response of the diaphragm is amplified significantly.

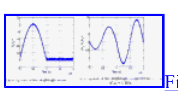
Figure 4.

To better understand the reason of this interesting behavior of the diaphragm, we investigate the effect of the fundamental natural frequency of the PCB and the shock pulse duration. Figure 5 shows the maximum normalized relative amplitude of the diaphragm for different ω_P values for shock duration ranging from 60 μs to 6.0 ms, which spans the practical experimental values [2]. Selected points in Figs. 5(b)5(c) were verified in Fig. 6 using ANSYS software [38]. The element COMPIN14 was used to model the springs and the structural mass element was used to model the masses. The F command was used to apply a half-sine input force directly to the PCB. The two figures show good agreement between the 2DOF model and the ANSYS model.

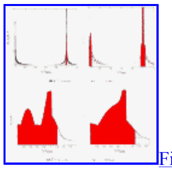
Figure 5.
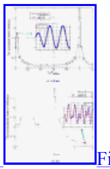
Figure 6.

Figure 5 indicates that the diaphragm response is amplified for specific zones of ω_P, shown in shaded areas, where the normalized response exceeds unity. The width of these frequency bands depends strongly on the shock duration values. For the case of T=6.0 ms, there are two narrow zones corresponding to ω_P=0.0 Hz–1.2 kHz and ω_P=23 kHz–25 kHz. As T decreases, the width of the two zones increases and they approach each other. Eventually, they merge into one zone, as depicted in Figs. 5(c)5(d). As noted from Fig. 5 there are three primary variables governing the behavior of the microstructure: T, ω_P, and ω_{MEMS}.

To span completely the design space of a microstructure, a 3D plot needs to be generated accounting for these variables. Figure 7 depicts an example of such for the studied diaphragm. The figure shows the maximum normalized response of the diaphragm relative to that of the PCB for different ω_P and shock pulse frequency ω_{Pulse} values. Here, only the magnitude of the displacement is shown, regardless of its sign. Figure 7(a) is for the case of $\omega_P/\omega_{\text{MEMS}}<1$ and Fig. 7(b) is for the case of $\omega_P/\omega_{\text{MEMS}}>1$. The diagram is split into two parts because the response is infinite (no damping) when the value of $\omega_P/\omega_{\text{MEMS}}$ is equal to 1.

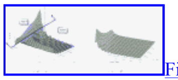
Figure 7.

In summary, Figs. 5,7 show that when the shock pulse duration is approximately larger than 0.1 ms, two small zones, where the diaphragm response is amplified, are defined. However, when the shock duration is approximately less than 0.1 ms, the two regions merge into one large region. Next we explore these two cases in more depth.

A1.Case 1. The diaphragm response in this region is amplified within two zones (Figs. 5(a)5(b)). The first zone is defined when the PCB experiences the shock load as a dynamic load (its natural period is close to the shock duration). The second zone is defined when the fundamental natural frequency of the PCB coincides with that of the microstructure. The span of the two zones decreases as the shock duration increases.

A2.Case 2. In this region, the two zones in Case 1 are merged into one zone. The reason behind this merging is that the shock duration value is very small in this region. Hence, the frequency band at which the PCB amplifies the input shock is increased. To clarify this merging more, we show in Fig. 8 the maximum normalized amplitude of the PCB response for different ω_P values for shock durations of T=1.0 ms and T=0.1 ms. It is clear from the figures that as the shock duration value decreases the span at which the PCB response will be amplified is increased. Hence, this will widen the frequency band of the amplified response of the microstructure. Interestingly, for this case, the diaphragm response to a shock load might exceed significantly the equivalent static deflection of the same shock load (although we are away from the traditionally known as resonance condition, which occurs when $\omega_P=\omega_{\text{MEMS}}$). For example, Fig. 9 shows the time history for the normalized diaphragm response relative to the PCB when T=60 μs and ω_P=19.2 kHz where its maximum value exceeds three times the corresponding static deflection of the diaphragm.

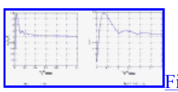
Figure 8.
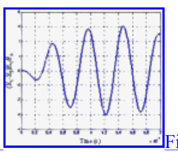
Figure 9.

B.Damped Response. Next, we investigate the light damping effect on the response of the diaphragm under shock loads. Figure 10 shows a 3D plot representing the maximum relative normalized diaphragm response in the case of a damping ratio ζ=0.05, for different ω_P and ω_{pulse}. Figures 11(a)11(b) show the maximum normalized relative amplitude of the diaphragm for different ω_P values for shock durations of 1.0 ms and 60 μs. The figures indicate that damping has a significant effect on the amplification zone that corresponds to the coincidence of the natural frequencies of the microstructure and the PCB, while it has much less effect on the zone where the PCB experiences the shock as a dynamic load.

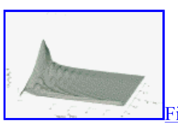
Figure 10.
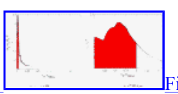
Figure 11.

The previous results (Figs. 4,5,6,7,8,9,10,11) indicate that neglecting the motion effect of a PCB, which represents one of the MEMS packaging levels, Fig. 1, on the response of a microstructure during shock may lead to amplification of its response. This is contradictory to what has been mentioned in literature that the worst-case scenario for the effect of the package is to merely transfer the shock pulse to the microstructure without significantly altering its shape or intensity [2]. Further, Figs. 5,11 show that designing the package or the PCB to have a much lower natural frequency than the microstructure, while attempting to separate the frequency of the microstructure from the PCB, may also result in amplification for the shock force affecting it.

C.Comparison Between a Continuous-Lumped Model With the 2DOF Model of a Clamped-Clamped Beam. In a previous work [19] we developed a continuous model of a clamped-clamped microbeam that is coupled with a lumped mass model of the PCB. Here we compare the results obtained of the 2DOF model with the model of Ref. [19]. To this end, the effective stiffness of the clamped-clamped beam is obtained according to the following equation:

$$k=\frac{32Ebh^3}{L^3} \qquad (8)$$

Figures 12,13 compare the results of the model in Ref. [19] with the 2DOF model results when the shock duration values are 1.0 ms and 0.1 ms, respectively. The figures show that the results are in good agreement. It is worth to mention here that in these figures, the effects of geometric nonlinearity of the continuous-lumped model has been neglected to enable comparison with the 2DOF model. This puts some limitation on the use of the 2DOF model to represent clamped-clamped beams and other structure suffering nonlinear behaviors. Also other limitations of the 2DOF include neglecting the fact that the PCB is a flexible structure that has an infinite number of modes of vibrations. These modes of vibration are expected to have an effect on the microstructure response if their natural period values are within the shock duration value. However, a clear advantage of the 2DOF model is its flexibility and ability to describe many microstructures, not only beams, which can be of irregular shapes.

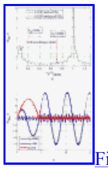Figure 12. 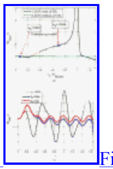Figure 13.

Effect of Electrostatic Forces

Here, we study the combined effect of assembly and electrostatic force on the response of the diaphragm to shock loads. In this investigation, we use a SIMULINK model [39] to tackle the nonlinear electrostatic force and integrate the equations of motions numerically with time. Here the system is governed by Eq. (1); however, the forcing term becomes

$$F(t) = \left[\frac{\varepsilon A V_{\mathrm{dc}}^2}{2(d - x_r)^2}, F_0[\sin(\omega_{\mathrm{pulse}} t)u(t) + \sin\ \omega_{\mathrm{pulse}}(t-T)u(t-T)]\right] \quad (9)$$

where x_r is the relative deflection of the diaphragm, V is the dc polarization voltage, A is the area of the diaphragm cross section, d is the capacitor gap width between the diaphragm and the stationary electrode on the PCB, and ε is the dielectric constant of the gap medium. The diaphragm has $A=1\times1$ mm^2. In the following analysis we assume complete overlapping between the two electrodes of the diaphragm.

Figure 14(a) shows the relative normalized response of the diaphragm to a shock pulse acceleration of amplitude 1000 g and T=0.25 ms. We assume a voltage load $V_{\mathrm{dc}}=31$ V and a PCB fundamental natural frequency 28.8 kHz. The figure indicates that the diaphragm has a stable response. On the other hand, Fig. 14(b) shows the diaphragm response to the same shock pulse but with a voltage value of 27 V and ω_P=1.92 kHz. Although in the latter case the electrostatic force is less than the first case, the diaphragm exhibit pull-in (unstable response). This can be justified by the fact that, according to Figs. 5,7, the small natural frequency of the PCB amplifies the shock loads on the diaphragm.

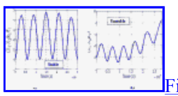Figure 14.

Figure 15 compares the pull-in voltage for the diaphragm against the shock amplitude of a half-sine pulse when modeling the diaphragm alone (without the PCB) (dashed) and with the PCB effect included (solid). We assume T=0.25 ms and ω_P=2.64 kHz. Here, also it is noted that the 2DOF model shows an earlier pull-in compared to the 1DOF model. The above results indicate the importance of modeling the effect of the PCB motion on electrostatic MEMS. By neglecting the effect of the PCB, there is a possibility that the device will fail to function properly and it might collapse and fail mechanically.

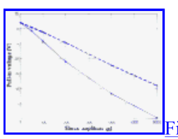Figure 15.

Summary and Conclusions

We investigated the response of MEMS devices under shock loads including the effect of the PCB motion. We used a 2DOF model for this investigation. A pressure microphone employing a microdiaphragm was chosen as the case study. We studied the effects of the fundamental natural frequency of the PCB, electrostatic force, damping, shock pulse duration, and their interactions. It was found that neglecting the PCB effect on the modeling of MEMS under shock loads can lead to erroneous predictions of the microstructure motion, especially for two cases: when the PCB experiences the shock load as a dynamic load and when the natural frequency of the PCB approaches that of the microstructure. The response is also found to depend strongly on the shock duration values.

Contradictory to what is mentioned in literature that a package, as a worst-case scenario, transfers the shock pulse to the microstructure without significantly altering its shape or intensity, we showed that a poor design of the package (PCB) might result in severe amplification of the shock effect. This amplification can cause early pull-in instability for MEMS devices employing electrostatic forces.

Future Work

As a future plan, more work is needed to verify experimentally the impact shock load effects. An experimental setup consisting of a hammer, an accelerometer, different PCB designs, and a differential laser vibrometer that has the ability to read two different measurement points at the same time can be used for this purpose. The hammer will be used to hit the PCB to simulate an impact shock load, and the differential laser will be used to read the MEMS and the PCB responses simultaneously. However, since controlling the hammer impact and using two laser readout systems might be difficult, it might be easier to design a base-excitation shock load using a well controllable shaker. This excitation method is found to share many similarities with the single point force assumed in this study. The theoretical and experimental work due to base excitation shock will appear in Ref. [34]. As an example, Fig. 16 shows one of the obtained results for a real MEMS device response with and without the PCB under base shock excitation [34].

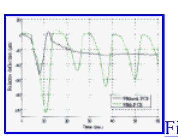Figure 16.

Acknowledgment

This work has been supported by NSF Award No. 0700683.

REFERENCES

1. Alajoki, M., Nguyen, N., and Kivilahti, J., 2005, "Drop Test Reliability of Wafer Level Chip Scale Packages," *Proceedings of 55th Electronic Components and Technology Conference*, Lake Buena Vista, FL, Vol. 1, pp. 637–644. first citation in article
2. Srikar, V., and Senturia, S., 2002, "The Reliability of Microelectromechanical Systems (MEMS) in Shock Environments," J. Microelectromech. Syst., **11**(3), pp. 206–214. [Inspec] first citation in article
3. Fan, M. S., and Shaw, H. C., 2001, "Dynamic Response Assessment for the MEMS Accelerometer Under Severe Shock Loads," National Aeronautics and Space Administration NASA, Report No. TP-2001-209978. first citation in article
4. Chang, H., Qian, J., Cetiner, B., Flaviis, F., Bachman, M., and Li, G., 2005, "Design and Processes Consideration for Fabrication RF MEMS Switches on Printed Circuit Boards," J. Microelectromech. Syst., **14**(6), pp. 1311–1322. [Inspec] first citation in article
5. Ghaffarian, R., Sutton, D., Chaffee, P., Marquez, N., Sharma, A., and Teverovsky, A., 2002, "Thermal and Mechanical Reliability of Five COTS MEMS Accelerometers," NASA Electronic Parts and Packaging Program, http://nepp.nasa.gov/eeelinks/February2002/Thermal_and_Mechanical_Reliability.pdf first citation in article
6. Ken, G., 2000, "MEMS PCB Assembly Challenge," Circuits Assem., **11**(3), pp. 62–70. first citation in article
7. Gogoi, B., Vujosevic, M., and Petrovic, S., 2000, "Challenges in MEMS Packaging," Proceedings of the SMIT International Conference, Rosemont, IL, pp. 775–783. first citation in article
8. Beeby, S., Ensell, G., Kraft, M., and White, N., 2004, *MEMS Mechanical Sensors*, Artech House, Boston, MA. first citation in article
9. Bigdeli, S., 2003, "Material and Reliability Requirements for MEMS Packaging" Project, Santa Clara University, http://www.sjsu.edu/faculty/selvaduray/page/papers/mate234/soheilbigdeli.pdf. first citation in article
10. Wagner, U., Franz, J., Schweiker, M., Bernhard, W., Muller-Fiedler, R., and Paul, O., 2001, "Mechanical Reliability of MEMS-Structures Under Shock Loads," Microelectron. Reliab., **41**, pp. 1657–1662. [Inspec] first citation in article
11. Li, G., and Shemansky, F., Jr., 2000, "Drop Test Analysis on Micro-Machined Structures," Sens. Actuators, A, **85**, pp. 280–286. [Inspec] first citation in article
12. De Coster, J., Tilmans, H., Van Beek, J., Rijks, G., and Puers, R., 2004, "The Influence of Mechanical Shock on the Operation of Electrostatically Driven RF-MEMS Switches," J. Micromech. Microeng., **14**(9), pp. S49–S54. [Inspec] first citation in article
13. Younis, M. I., Miles, R., and Jordy, D., 2006, "Investigation of the Response of Microstructures Under the Combined Effect of Mechanical Shock and Electrostatic Forces," J. Micromech. Microeng., **16**, pp. 2463–2474. [Inspec] first citation in article
14. Younis, M. I., Alsaleem, F., Miles, R., and Su, Q., 2007, "Characterization of the Performance of Capacitive Switches Activated by Mechanical Shock," J. Micromech. Microeng., **17**, pp. 1360–1370. first citation in article
15. Younis, M. I., Jordy, D., and Pitarresi, J., 2007, "Computationally Efficient Approaches to Characterize the Dynamic Response of Microstructures Under Mechanical Shock," J. Microelectromech. Syst., **16**, pp. 628–638. first citation in article
16. Jiang, Y., Du, M., Huang, W., Xu, W., and Luo, L., 2003, "Simulation on the Encapsulation Effect of the High-g Shock MEMS Accelerometer," *Proceedings of the Fifth International Conference on Electronic Packaging Technology*, Vol. 28, pp. 52–55. first citation in article
17. Shetye, D. M., 2004, "Drop Response of a Silicon Microacoustic Sensor," MS thesis, State University of New York at Binghamton, Vestal, NY. first citation in article
18. Bart, S., Zhang, S., Rabinovich, V., and Cunningham, S., 1999, "Coupled Package-Device Modeling for MEMS," Proceedings of MSM 99, San Juan, PR. first citation in article
19. Younis, M. I., Al Saleem, F., and Jordy, D., 2007, "The Response of Clamped-Clamped Microbeams Under Mechanical Shock," Int. J. Non-Linear Mech., **42**, pp. 643–657. [Inspec] first citation in article
20. Suhir, E., 2005, "Structural Analysis of Microelectronic and Photonic Systems," Proceedings of ASME/Pacific Rim Technical Conference and Exhibition on Integration and Packaging of MEMS, NEMS, and Electronic Systems: Advances in Electronic Packaging, pp. 907–919. first citation in article
21. Steinberg, D. S., 2000, *Vibration Analysis for Electronic Equipment*, 3rd ed., Wiley Interscience, New York. first citation in article
22. Suhir, E., and Burke, R., 1994, "Dynamic Response of a Rectangular Plate to a Shock Load, With Application to Potable Electronic Products," IEEE Trans. Compon., Packag. Manuf. Technol., Part B, **17**(3), pp. 449–460. [Inspec] [ISI] first citation in article
23. Suhir, E., 2002, "Could Shock Tests Adequately Mimic Drop Test Conditions?," ASME J. Electron. Packag., **124**(3), pp. 170–177. [ISI] first citation in article
24. Pitarresi, J. M., and Primavera, A., 1992, "Comparison of Modeling Techniques for the Vibration Analysis of Printed Circuit Cards," ASME J. Electron. Packag., **114** (4), pp. 378–383. first citation in article
25. Suhir, E., 1996, "Dynamic Response of a One-Degree-of-Freedom Linear System to a Shock Load During Drop Tests: Effect of Viscous Damping," IEEE Trans. Compon., Packag. Manuf. Technol., Part A, **19**(3), pp. 435–440. [Inspec] [ISI] first citation in article
26. Suhir, E., 1992, "Nonlinear Dynamic Response of a Printed Circuit Board to Shock Loads Applied to Its Support Contour," ASME J. Electron. Packag., **114**(4), pp. 368–377. first citation in article
27. Wong, E. H., 2005, "Dynamics of Board-Level Drop Impact," ASME J. Electron. Packag., **127**(3), pp. 200–207. [ISI] first citation in article
28. Keltie, R. F., Falter, K. J., 1993, "Guidelines for the Use of Approximations in Shock Response Analysis of Electronic Assemblies," ASME J. Electron. Packag., **115** (1), pp. 124–130. first citation in article
29. Wong, E. H., Mai, Y. W., and Seah, S. K., 2005, "Board Level Drop Impact: Fundamental and Parametric Analysis," ASME J. Electron. Packag., **127**(4), pp. 496–502. first citation in article
30. Dally, J. W., 1990, *Packaging of Electronic System, A Mechanical Engineering Approach*, McGraw-Hill, New York. first citation in article
31. Hernried, A. G., and Sackman, J. L., 1968, "The Two-Degree-of-Freedom Equipment Structure System," ASME J. Electron. Packag., **112**(6), pp. 621–628. first citation in article
32. Abdel-Rahman, M., Younis, M. I., and Nayfeh, A. H., 2002, "Characterization of the Mechanical Behavior of an Electrically Actuated Microbeam," J. Micromech. Microeng., **12**, pp. 795–766. [Inspec] first citation in article
33. Hernried, A. G., and Sackman, J. L., 1968, "The Two-Degree-of-Freedom Equipment Structure System," J. Micromech. Microeng., **112**(6), pp. 621–628. first citation in article
34. Alsaleem, F. M., Younis, M. I., and Ibrahim, M., "A Study for the Effect of the PCB Motion on the Dynamics of MEMS Devices Under Mechanical Shock," J. Microelectromech. Syst, submitted. first citation in article
35. Harris, C. M., 2002, *Shock and Vibration Handbook*, 5th ed., McGraw-Hill, New York. first citation in article
36. Lalanne, C., 2002, *Mechanical Vibration and Shock: Mechanical Shock Volume*, Hermes Penton Ltd., London. first citation in article
37. Cui, W., 2005, "Analysis, Design and Fabrication of a Novel Silicon Microphone," Ph.D. thesis, State University of New York at Binghamton, Vestal, NY. first citation in article
38. www.ANSYS.com first citation in article
39. The MathWorks, available at http://www.mathworks.com/ first citation in article

FIGURES

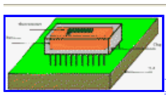
Full figure (11 kB)

Fig. 1 Schematic of the assembly (packaging) levels of a MEMS device First citation in article

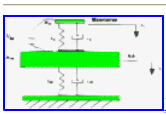
Full figure (8 kB)

Fig. 2 A 2DOF model of a microstructure mounted on a PCB First citation in article

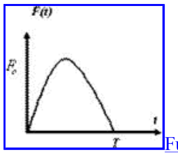Full figure (4 kB)

Fig. 3 Schematic of a half-sine pulse used to model actual shock loads First citation in article

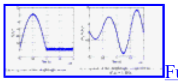Full figure (21 kB)

Fig. 4 Time history for the normalized displacement of the diaphragm for a half-sine pulse of T=1.0 ms First citation in article

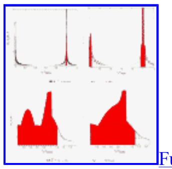Full figure (34 kB)

Fig. 5 The maximum normalized relative amplitude of the diaphragm for different ω_p values. The results are shown for a half-sine pulse for the case of no damping. First citation in article

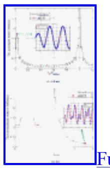Full figure (28 kB)

Fig. 6 A comparison of the microstructure response to impact shock load using ANSYS and the modal analysis solution First citation in article

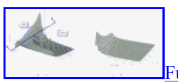Full figure (29 kB)

Fig. 7 The maximum normalized relative amplitude of the diaphragm for different ω_p and ω_{pulse} values First citation in article

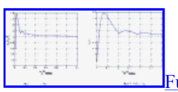Full figure (22 kB)

Fig. 8 The maximum normalized amplitude of the PCB response for different ω_p values First citation in article

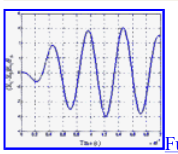Full figure (18 kB)

Fig. 9 Time history for the normalized relative displacement of the diaphragm when ω_p=19.2 kHz and T=60 μs First citation in article

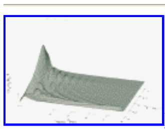Full figure (18 kB)

Fig. 10 The maximum normalized relative amplitude of the diaphragm for different ω_p and ω_{pulse} values when ζ=0.05 First citation in article

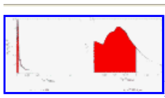Full figure (15 kB)

Fig. 11 The maximum normalized relative amplitude of the diaphragm for different ω_p values when ζ=0.05 First citation in article

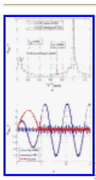Full figure (32 kB)

Fig. 12 The response of the MEMS-PCB assembly to an impact shock load of shock duration T=1 ms: (a) response spectrum and (b) transit response for the continuous-

lumped model [19] First citation in article

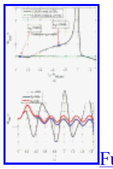
Full figure (29 kB)

Fig. 13 The response of the MEMS-PCB assembly to an impact shock load of shock duration $T=0.1$ ms: (*a*) response spectrum and (*b*) transit response for the continuous-lumped model [19] First citation in article

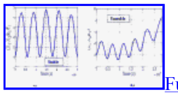
Full figure (26 kB)

Fig. 14 Time history for the normalized relative response of the diaphragm to a half-sine pulse of $T=0.25$ ms, showing (*a*) a stable response when $\omega_P=28.8$ kHz and $V_{dc}=31$ V, and (*b*) a pull-in state (unstable response) when $\omega_P=1.92$ kHz and $V_{dc}=27$ V First citation in article

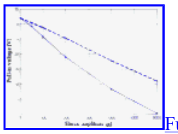
Full figure (22 kB)

Fig. 15 A plot of the pull-in voltage of the diaphragm against shock load amplitude of a half-sine pulse, accounting for the PCB motion (solid) and neglecting the PCB motion (dashed). The results are shown for the case $T=0.25$ ms and $\omega_P=2.64$ kHz. First citation in article

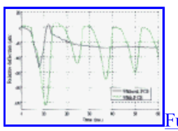
Full figure (14 kB)

Fig. 16 The transient response of a capacitive MEMS device with and without a PCB when subjected to base shock load generated by a controllable shaker, as monitored through a laser doppler vibrometer ($T=5.0$ ms, and the ratio between the natural frequency of the PCB to the MEMS is 1.24) [34] First citation in article